

# Estimation of overpressures from porosity based method : a theoretical approach applied to the central/coastal swamp depo-belts of the Niger delta basin

Mkpese, Ubon Udofia \*

Department of Physics, University of Port Harcourt, Rivers State, Nigeria

\*Corresponding author E-mail: [ubon.mkpese@gmail.com](mailto:ubon.mkpese@gmail.com)

## Abstract

The Depth-dependent compaction theory that variations in certain geophysical properties with depth; bulk density, formation resistivity together with sonic velocity being a reflection of the pressure regime is the basis for pore pressure prognosis study. Pore pressure prediction (PPP), when done accurately can be used to avert disaster and helps in safe drilling. A porosity-based model has been applied to predict overpressured zones in an onshore environment of the Niger delta basin. Zones with hard overpressures greater than a magnitude of 0.7 psi/ft are generally within 10000ft and below. Top of overpressures for studied wells ranges between 7000ft and 10000ft. Porosities in shale are of typical values ranging between 0.05 to 0.46. A robust concordance between PPP and MPP profiles for each of the wells validates the results here and confirms suitability of model to the studied area.

**Keywords:** *Compaction Disequilibrium; Normal Compaction; Overpressure Mechanism; Shale Trend; Niger Delta.*

## 1. Introduction

Abnormal formation pressures would usually pose a major challenge to drillers and as such is one area that requires careful and in-depth studies. Such case scenario where fluid pressure within the pore exceeds, in the significant amount, or is below that of the normal pressure (the hydrostatic pressure) at a particular depth of consideration is said to be abnormal (Jiao *et al.*, 1998). More cases of overpressures rather than underpressures have been reported in sedimentary basins around the world. Predictions of abnormal pore pressures are done using well logs or seismically derived velocities or both integrated (Kumar *et al.*, 2012; Ugwu, 2015)

In normally compacted sediments, porosity decreases with depth in an exponential order leading to an increase in sonic velocity, assuming no significant rock type variations. However, if a rock formation is over pressured at some depth, then the high pressure of the pore fluid retards compaction and keeps the porosity high. This consequentially affects the geophysical parameters of rock, producing observable departures from expected trends: lower densities, slower velocities and lower resistivity than expected. Hence, Overpressure detection is built on the compaction-dependent theory that geophysical properties would reflect formation pressure. Shales are the lithologies of preference in pressure interpretation since they respond better to overpressure than other rock types, especially in where it is extremely a sand/shale formation. Consequently, detection of overpressure is concentrated on shale deformation behaviors.

For accurate prediction, appropriate models must be selected. They have been propositioned of several of such prediction models in recent years. These are based either on graphical extrapolation, velocity calibration or empirical power laws. Among such models, the most widely used throughout the industry are the Eaton's method (Eaton, 1975) and Bowers' method (Bowers,

1995). Porosity based model proposed in (Zhang, 2011) has been adopted throughout this work. We note, however, that the choice of any prediction model for any sedimentary basin is dependent not only on the causal mechanism of overpressure but also on the researcher's experience (Zijian, 2015).

### 1.1. Objectives of study

This study is aimed at applying a porosity-based model (Zhang, 2011) to estimate overpressures in parts of the Niger Delta basin. Objectives are to:

- 1) Carry out density vs. P-wave velocity analysis in order to determine the mechanism(s) that generates overpressures in the study area.
- 2) Estimate shale formation porosities in the study area.
- 3) Estimate overpressures within the sediments of study locations using porosity based pore pressure prediction (PPP) model
- 4) Compare the predicted overpressures obtained within the shale zones to measured pore pressures (MPPs).

### 1.2. Geologic setting and location of study area

The Niger Delta is one of the largest sub-aerial basins in Africa having a sub-aerial section of about 75, 000km<sup>2</sup>, area measuring about 300, 000km<sup>2</sup>, and with sediment thickness of about 500, 000km<sup>3</sup>. The thickness of the sediments varies between 9to12km. Large-scale tectonics of the area must have resulted to different complexities in the geologic formation (Tuttle *et al.*, 2015).

Three main lithostratigraphic formations have been identified and classified accordingly as being "Continental," "Transitional" and "Marine" depositional environments, which correspond to the Benin formation on the top, the Agbada formation in-between and the Akata formation at the bottom (Short and Stauble, 1967).

**Akata Formation:** This sedimentary unit is at the base and composes mostly of the marine shales. These shales are under compacted and most probably contain “abnormally high-pressured” siltstones or fine-grained sandstones. It is believed by many to be the main source rock for the Delta’s hydrocarbon and the basic unit of the Cenozoic complex. The Akata formation has a thickness between 0.6km to 6km and has been speculated as being the major source bed for hydrocarbon.

**Agbada Formation:** This formation which is believed to be the main hydrocarbon habitat of the basin has a thickness varying between 2.8km and 4. 2km. It is dominated extremely by sand/shale alternations. The sands, although consolidated, have a matrix that is calcareous in nature; the sediments are aged between mid-Miocene to be late-Miocene.

**Benin Formation:** The formation has a thickness up to 3km and consists of predominantly sandstone sequence intercalated with a few shale, which increases in proportion as you drill down deep. The upper continental plane of the deltaic environment fed the sand deposited in the formation in large proportion. Sediments of the formation range in age from Oligocene geologic age in the northern section to their Recent equivalent in today Delta.

The location map of the studied wells is displayed in Fig. 1. Only surface locations are shown; deviations not illustrated. The wells are all from the central/coastal swamp depositional belts of the Niger Delta (Doust and Omatsola, 1990).

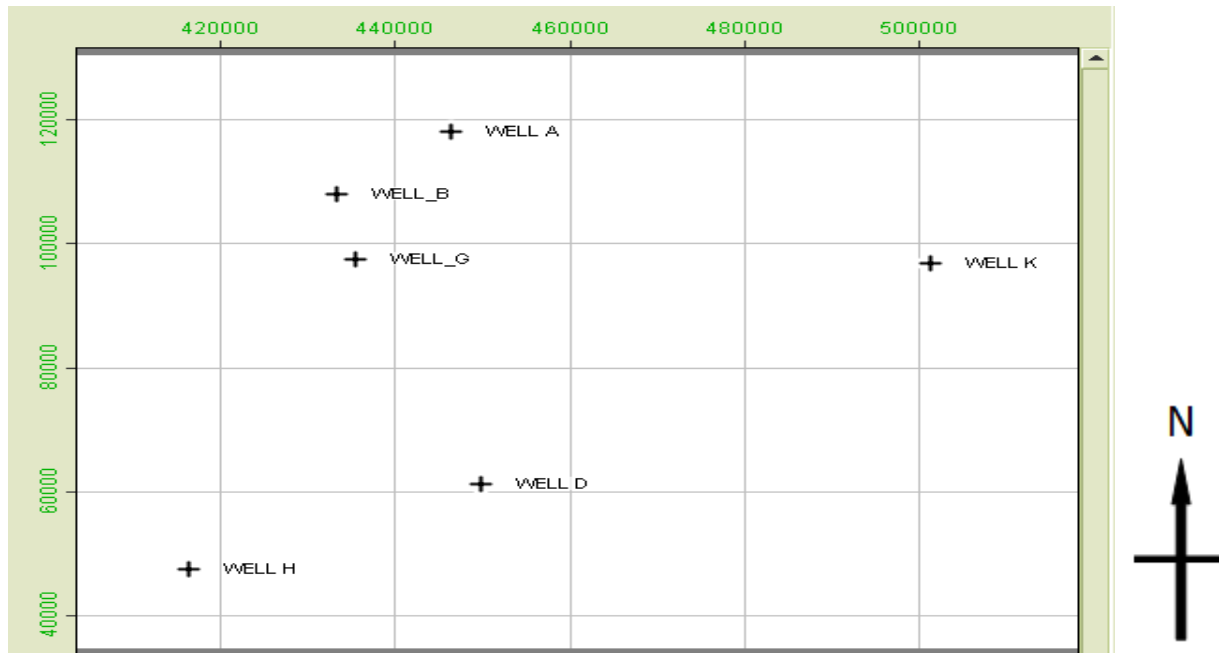


Fig. 1: Studied Wells Located Within the Central/Coastal Swamp Depo-Belts of the Niger Delta Basin.

## 2. Basic concepts of pressure

The term pressure is most commonly associated with fluids just as force is used with solid matter. Pore pressure also called “formation pressure”,  $P_p$ , is the pressure which acts on the pore fluids of a rock formation. Hydrostatic pressure,  $P_h$ , refers to the pressure resulting from the fluid weight in a column:

$$P_h = \rho_f g z \quad (1)$$

Where,  $\rho_f$  and  $g$  are the column height, density of fluid, and gravitational acceleration respectively. At any depth, the normal hydrostatic pressure is defined as the formation pressure that is equals the hydrostatic pressure resulting to a (open) column of pore fluids that reaches to the vertical depth of considered formation from surface. In formations with normal pressures, pore fluids communicate efficiently with surface during burial. Therefore, the fluids in the pore spaces are squeezed out following normal compaction rate and results to hydrostatic pressure regime. Meanwhile the lithostatic (overburden pressure),  $S$ , is the pressure resulting from weight of rock matrix and pore fluids combined that is overlying the formation of consideration. Mathematically, this is written as (equation 2):

$$S = g \int_0^z \rho_b z dz \quad (2)$$

Where  $\rho_b$  is the bulk density dependent on depth and given by:

$$\rho_b = \phi \rho_f + (1 - \phi) \rho_{ma} \quad (3)$$

Where  $\phi$ ,  $\rho_f$  and  $\rho_{ma}$  are respectively the porosity, density of pore fluid and grain density or rock matrix density.

The resultant different between overburden pressure,  $S$ , and pore pressure  $P_p$  gives us the differential pressure or effective pressure and its acts on the rock matrix. This effective pressure is given as:

$$\sigma = S - \alpha P_p \quad (4)$$

The poro-elastic coefficient,  $\alpha$ , is introduced in Terzaghi’s original equation when applied to consolidated rock formation to take care decreasing effect in fluid pressure now applied on less of the grain surface. Generally,  $\leq 1$  but the values between 0.7 and 1.0 are commonly used. For overpressured rocks, is usually around 0.8 (Ugwu, 2015). The process of sediment compaction is actually controlled by the effective stress and as such if the effective stress is reduced in anyway, then compaction rate is slowed down. Fig. 2 illustrate the above assertion.

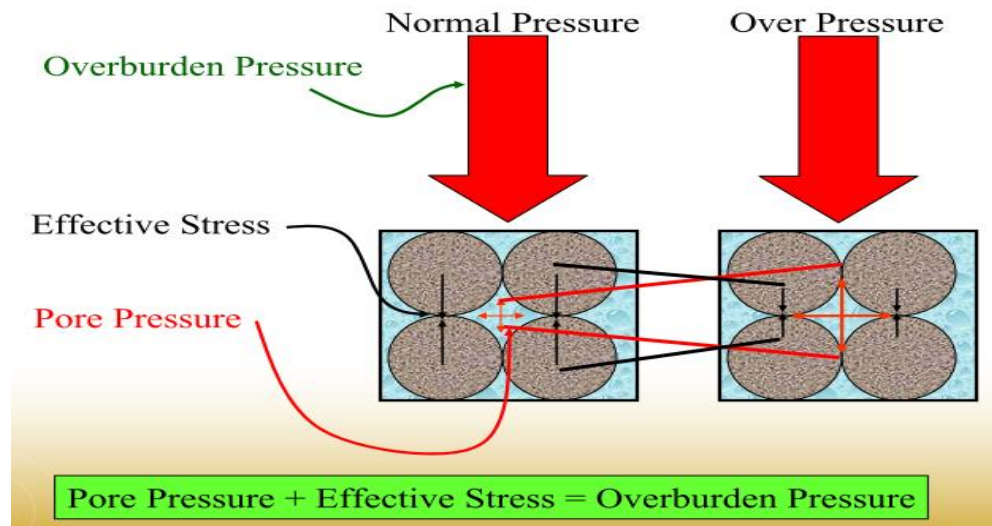


Fig. 2: Pictorial Representation of Terzaghi's Principle. (Kumar *et al.*, 2012)

## 2.1. Overpressure-generating mechanisms and identification methods

A variety of processes are postulated as causal process of overpressure generation; the most commonly quoted are reduction in porosity owing to compaction disequilibrium or lateral stresses, and fluid expansion. In the latter case, the excess fluid associated with hydrocarbon generation is considered to be a major contributor to overpressure building, particularly at depths greater than 3600m (12,000 ft) (Swarbrick and Osborne, 1998; Traugott, 1997).

Various authors (Bowers, 1995; Kumar *et al.*, 2012; Zhang, 2011) have been able to show that plotting certain petrophysical parameters together can provide useful information on overpressure mechanisms at play. The cross-plots of vertical effective stress and velocity (VES-Vp), vertical effective stress and density (VES-density), and velocity against density are effective analyzing tools for this purpose. Since compaction actually increases brings the grains of rock matrix much closer, it would then reduce porosity, increasing velocity and density as you go down deep. Disequilibrium compaction and secondary mechanisms derives their discriminating response based on the theory above. On the plots, disequilibrium compaction goes along the normal/virgin curve. Various overpressure mechanisms such as an unloading episode

can be identified when there is a significant deviation from the normal trend; the deviation can equally be a reflection of a change in shale composition.

## 2.2. Normal compaction trend in shale

The normal compaction trend (NCT) is a reflection of such properties like sonic velocity and resistivity values obtainable if the pore pressure were normal (hydrostatic). Lithologically identical rocks with equal values of properties at different depths have the same effective stress. The normal compaction trend depends on the variation of rock properties with depth of burial at a normal hydrostatic pressure. Particularly, the physical properties of shale depend primarily on the degree of compaction. In nature, the density, resistivity and/or porosity of normally, compacted rocks and burial depth have an exponential relationship. Plotting this relationship gives a very smooth curve called the normal compaction curve. Alternatively, the exponential dependencies are shown by straight lines if they were displayed on semi-logarithmic plots. Deviation from the smooth curve or the straight line would technically indicate an upper boundary called the top of geopressure zone. A typical NCT curve is shown in Fig. 3.

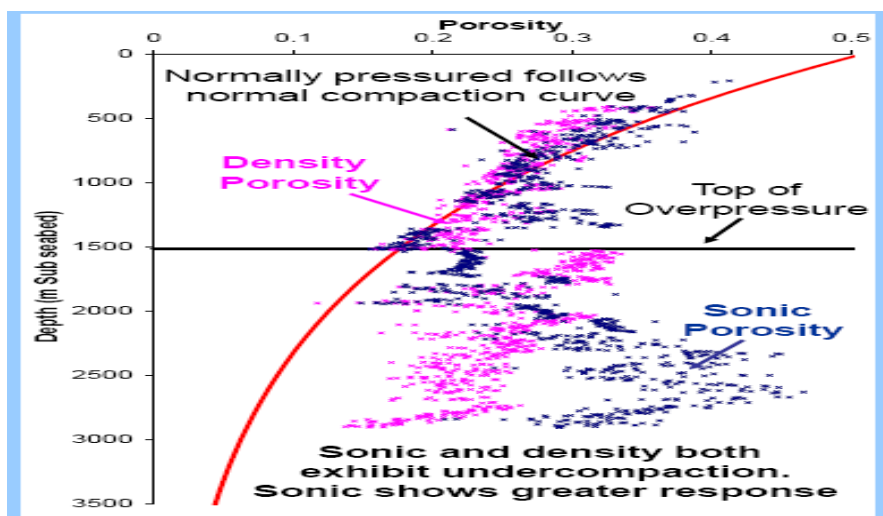


Fig. 3: An Example of the Normal Compaction Curve (Tingay *et al.*, 2009).

### 3. Materials and methods

Pore pressure prognosis studies yield results depending on the data quality used and the techniques applied. In this study, overpressured zones are predicted using petrophysical log data obtained from six (6) exploration wells in the Central/Coastal swamp depositional belts of the Niger Delta. The data were made available by Shell Petroleum Development Company (SPDC), Port Harcourt. Porosity based prediction model (Zhang, 2011) were applied on the RokDoc software. The model parameters were inputted to the software by means of log calculator function.

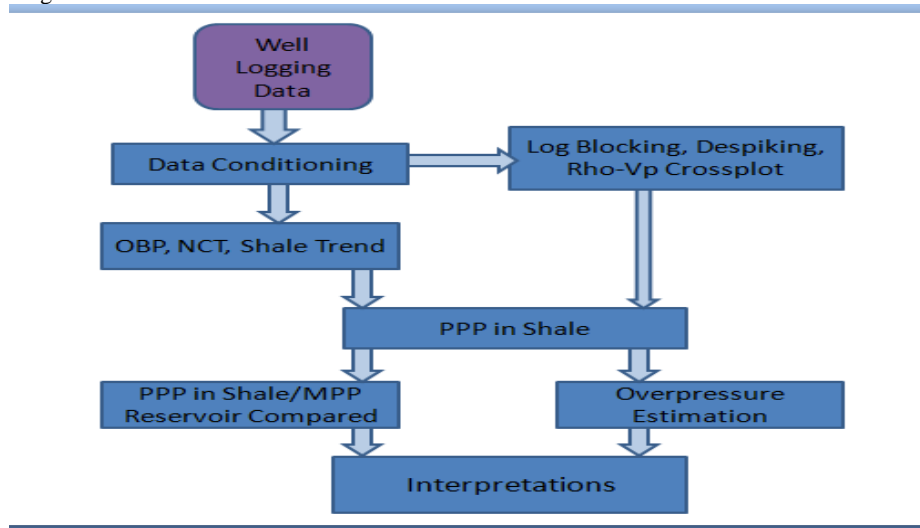


Fig. 4: Diagrammatic Workflow for Overpressure Prediction Studies.

#### 3.2. Porosity-based prediction model

A theoretical equation (Zhang, 2011) derived for pore pressure prediction (PPP) from porosity according to normal compaction trend of porosity. At any depth of interest,  $Z$  the expression for the pore pressure gradient is given as:

$$P_{pg} = S_g - (S_g - P_{hg}) \frac{\ln \phi_0 - \ln \phi}{cZ} \quad (5)$$

$S_g$ ,  $P_{hg}$ ,  $\phi_0$ ,  $\phi$  and  $c$  are, respectively, the lithostatic pressure gradient, hydrostatic pressure gradient, porosity in the mudline, porosity at depth of interest and compaction constant.

Several other predictions based on porosity exist (Flemings *et al.*, 2002; Holbrook *et al.*, 2005). However, the good thing about Zhang's calculated pressures from porosity model is its depth-dependent nature. In other words, the normal compaction trendline of porosity is not completely a constant but varies with depth or it is a function of depth. Overpressure sets in where porosity ( $\phi$ ) at an interested depth is greater than the normal porosity ( $\phi_n$ ) at the same depth. To determine the normal compaction trendline, equation (6) is applied:

$$\phi_n = \phi_0 e^{-cZ} \quad (6)$$

The theoretical equation is inputted into the RokDoc using the Log calculator function. The porosity logs were derived from "sonic-transit-time" using Wyllie's equation (Zhang, 2011).

$$\phi = \frac{\Delta t - \Delta t_{ma}}{\Delta t_f - \Delta t_{ma}} \quad (7)$$

Where  $\Delta t$  is the formation interval transit time (p-sonic log),  $\Delta t_{ma}$  is the matrix transit time and  $\Delta t_f$  is the interstitial fluids transit time.

To predict pressures from porosity, we need to generate porosity log. Suitable values of  $\Delta t_{ma}$  and  $\Delta t_f$  are chosen for better predic-

#### 3.1. Workflow for log-based overpressure prediction

Fig. 4 illustrates the workflow adopted for these studies. It begins with well log conditioning/editing, generation of Normal Compaction Trends (NCT), OverBurden Pressures (OBP), velocity/porosity trends in shales, Pore Pressure Prediction (PPP) in shales, comparison with Measured Pore Pressures (MPP) in adjacent reservoir zones and finally the interpretations.

tions. Conventional values are generally within 60 to 80  $\mu\text{s}/\text{ft}$  and 189 to 200  $\mu\text{s}/\text{ft}$  for  $\Delta t_{ma}$  and  $\Delta t_f$  respectively. The use of higher or lower values is prompted by lithology and pore fluid type (Carmichael, 1982). The porosity values generated are then used in constructing the normal compaction porosity trend (por\_NCT) and porosity in shale beds (por\_ShaleTrend). The por\_shaleTrend is input for calculating PPP from porosity.

### 4. Results and discussion

The study has identified tops of overpressures in the wells considered. A combination of basic input parameters; sonic logs, bulk density and shale volumes were used to generate normal compaction velocity and or porosity trends, shale porosity trends and shale velocity trends.

Six wells A, B, D, G, H and K representing Akaso, Gbaran, Santa Barbara, Kolo Creek, Elepa and Korokoro fields respectively are the case-studies; all from the Central/Coastal swamp depobelts of the Niger Delta basin. These wells were chosen because of the history of overpressures of their associated fields. Suitable transit times were inputted in the calculation of the porosities and compaction constant were computed from the constructed normal compaction porosity trends. The values for each well set are; WELL A ( $\Delta t_{ma} = 73 \mu\text{s}/\text{ft}$ ,  $\Delta t_{ma} = 200 \mu\text{s}/\text{ft}$ ,  $c = 0.00016 /\text{ft}$ ); WELL B ( $\Delta t_{ma} = 72 \mu\text{s}/\text{ft}$ ,  $\Delta t_{ma} = 224 \mu\text{s}/\text{ft}$ ,  $c = 0.00020$ ); WELL D ( $\Delta t_{ma} = 70 \mu\text{s}/\text{ft}$ ,  $\Delta t_{ma} = 219 \mu\text{s}/\text{ft}$ ,  $c = 0.00023$ ); WELL G ( $\Delta t_{ma} = 73 \mu\text{s}/\text{ft}$ ,  $\Delta t_{ma} = 237 \mu\text{s}/\text{ft}$ ,  $c = 0.00012$ ); WELL K ( $\Delta t_{ma} = 79 \mu\text{s}/\text{ft}$ ,  $\Delta t_{ma} = 239 \mu\text{s}/\text{ft}$ ,  $c = 0.00053$ ) and WELL H ( $\Delta t_{ma} = 73 \mu\text{s}/\text{ft}$ ,  $\Delta t_{ma} = 209 \mu\text{s}/\text{ft}$ ,  $c = 0.00042$ ). Mudline porosity value used for all studied wells is  $\phi_0 = 0.8$ .

#### 4.1. Preliminary results

To carry out 1-D PPP in shales, certain parameters have to be calculated or generated. In this category are presented results for such parameters which include shale volume ( $V_{shale}$ ), overburden pressure profile (OBP), Normal compaction trend (NCT), shale

velocity and porosity trends. Shale volume log represents the volume fraction of shale as measured or inferred from formation properties. During this study, the shale volume was calculated from Gamma ray log. Preliminary results were generated for all

the wells, including analysis for overpressure mechanism, but are presented only for well A (Fig. 5-8).

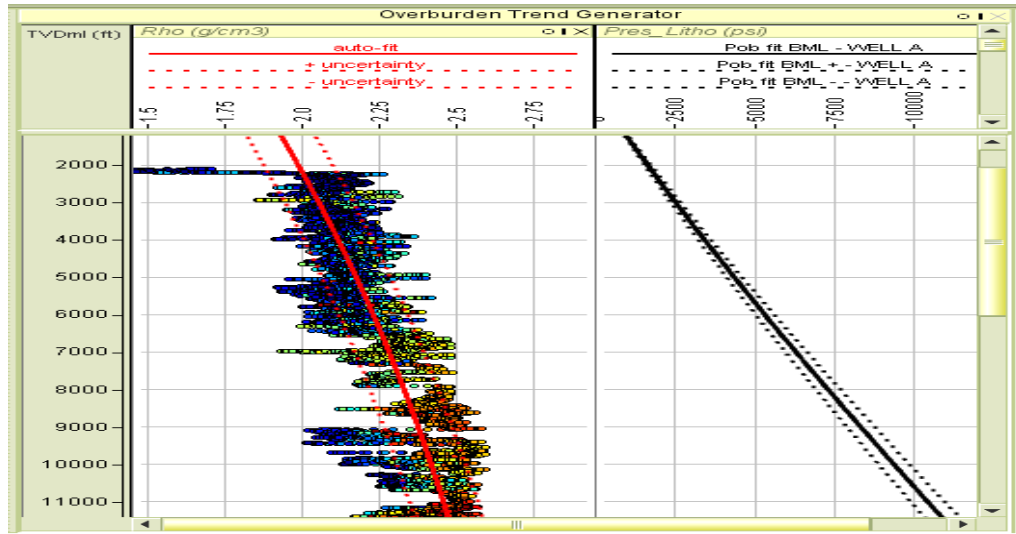


Fig. 5: Overburden (OVB) Trend and Rho Fit for Well A

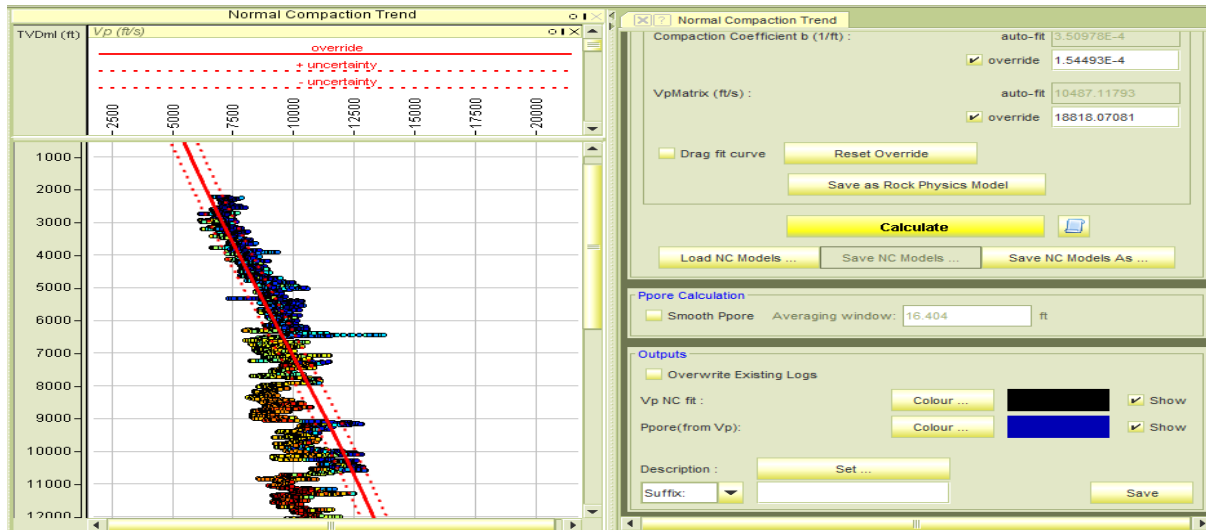


Fig. 6: Normal Compaction Trend and Line of Fit for Well A.

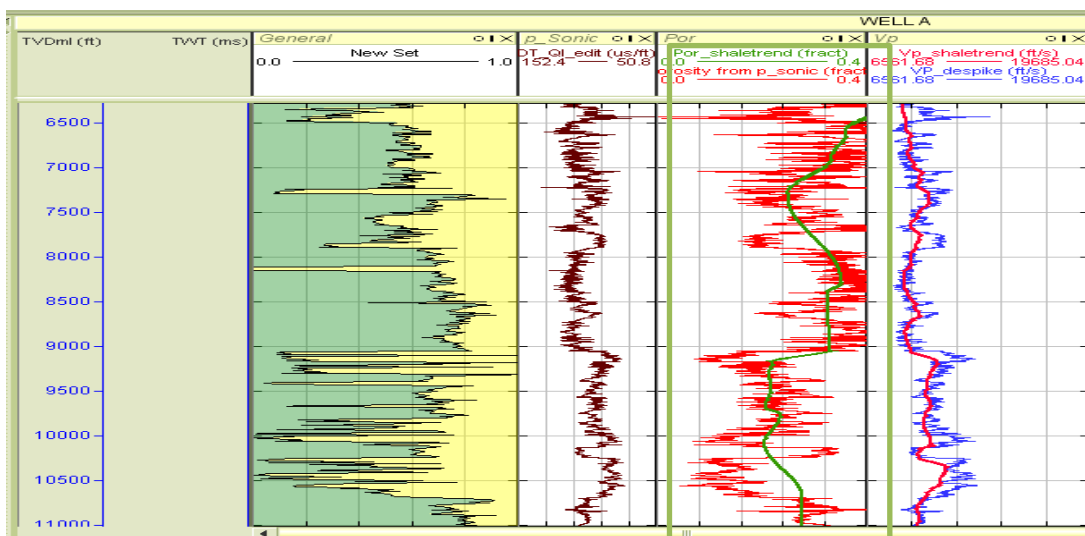


Fig. 7: Log Section (Volume of Shale, P-Sonic Log, Porosity, Shale Trend, Vp Shale Trend).

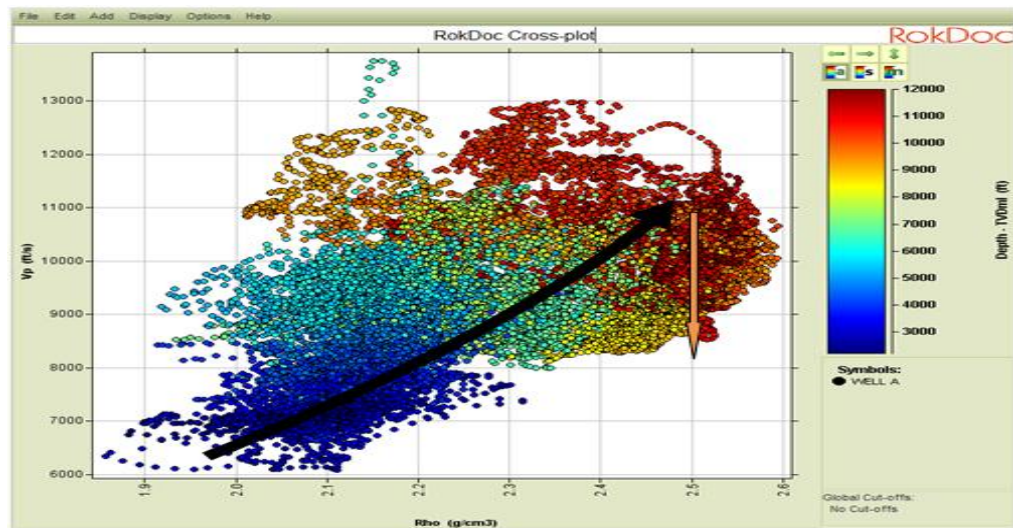


Fig. 8: Velocity vs. Density Cross-Plot for WELL A.

With an assumption that sediment compaction is directly proportional to the depth of burial and by proxy as well to the overburden stress, the velocity is considered to increase at a constant rate. So a normal compaction trend model is constructed from input log data of any type in this case; the Vp log and porosity log generated from sonic transit times (p\_sonic log) has been used. The workflow used in Rokdoc will also use the NCT to generate pore pressure profiles. A normal compaction trend model is calculated from input log data (NC fit). The NC fit is used together with the input log, hydrostatic pressure profile and lithostatic pressure profile to calculate a pore pressure log (Ppore) for each well and for each of the log input log type. An initial estimate of the normal compaction trend is done using a reciprocal input log transform.

#### 4.2. Numerical results

The calculated porosities in shale beds are presented in the tables 1 to 6 (refer to Appendix) respectively for the six well locations. Depth intervals of 200ft have been sampled; these are just representative depths since the work is not intended for detailed study of porosity. The porosity values in shales, measured as fractions, ranges from as low as 0.04 (4%) to as high values as 0.69 (69%). Higher values are closer to the surface. Depth zones with overpressures are associated with higher values of porosities (deviation from normal trend).

#### 4.3. Discussion/overpressured zones

Generally, results from all the wells indicate the presence of overpressured zones, hydrostatic formations and even zones characterized with certain degrees of underpressures. Top of overpressures are generally within depth of 6000ft to about 12500ft across all studied wells; mild overpressures are observed at shallow depths while hard overpressures occur at depths generally below 10000ft (TVDss) for all studied wells.

The result shows that well A (Fig. 9) maintains hydrostatic pressure mudline to a depth of about 7000ft where an onset of over-

pressure measuring between 0.55 and 0.60 psi/ft are predicted. The responses from “key logs” compared with standard models also confirm the presence of overpressures in the well. Robust matches also exist between the Measure Pressure (MPP) and Predicted Pressures at the well location, a result which approves the suitability of prediction model used.

At the well location, overpressure onset is observed beginning from about a depth of 8000ft. At this depth the predicted pressures begin to move away from normal hydrostatic line with log response also beginning to deviate from the normal compaction trendline at that depth, signifying onset of overpressure. Formation pressure gradient averaging about 0.65 psi/ft is observed; falling to the class called mild overpressure. The “mild overpressures” are seen continuing steadily down to about 11000ft beyond which “hard overpressures” measuring up to about 0.80psi/ft are observed.

Well B (Fig. 10) is characterized with hydrostatic pressure from the beginning to about 10500ft where very mild overpressure (<0.6psi/ft) sets in. Hard overpressures zone predicted at about a depth of 15500ft to about 16000ft where the well is terminated probably suggesting why the well is terminated at that depth (MPP values approaching lithostatic pressure). All PPPs from the “prediction models” each compares favorably with MPPs except at the terminating depths; an observation which cannot be resolved.

At well D (Fig. 11) location, similar result has been obtained at shallow depths as that in well B but slightly different at deeper zones. Hydrostatic pressure is observed until about 10000ft where an onset of mild overpressure begins. The zone between 13000ft and 15000ft can be referred to as a “wavy” pore pressure zone, since there are switches between overpressures and hydrostatic pressures at short intervals. This zone is a transition zone within which there are quick alternations between shale and sand beds before penetrating the thick shale bed just below the zone (below 15000ft) where the well is overpressured until last drilled depth.

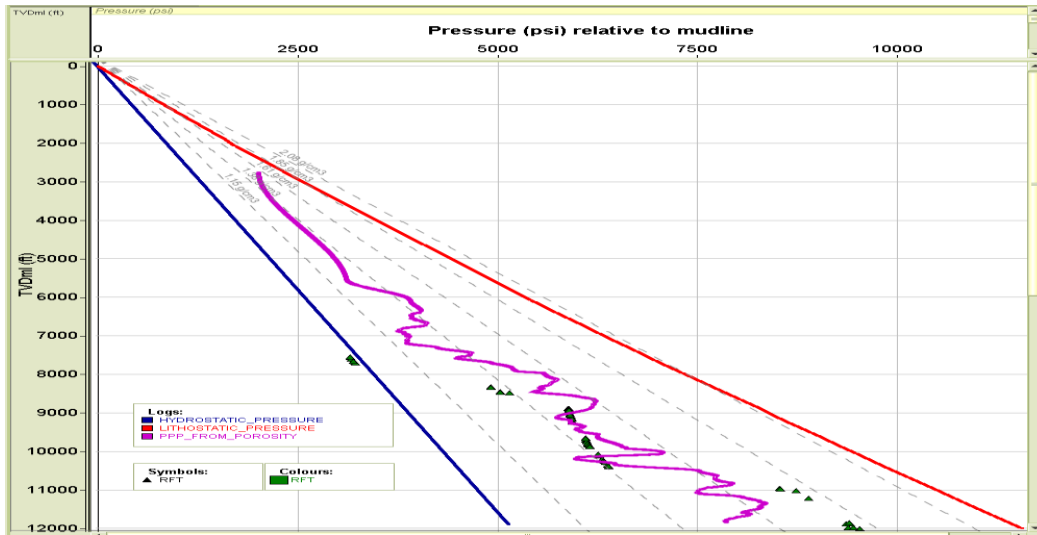


Fig. 9: Pressure Depth Plot Showing PPP from Porosity Model and MPP of Well A.

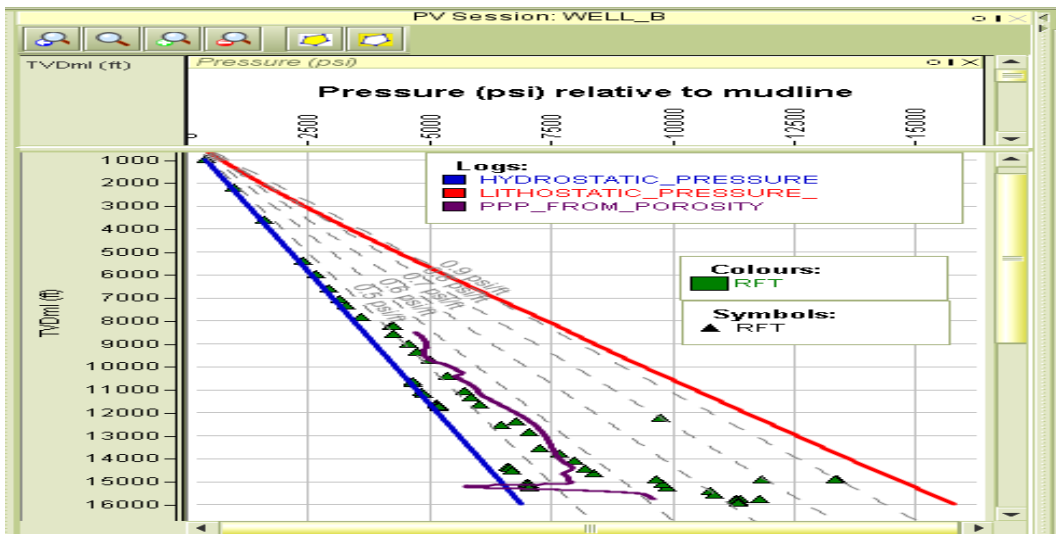


Fig. 10: PPP from Porosity Model for Well B.

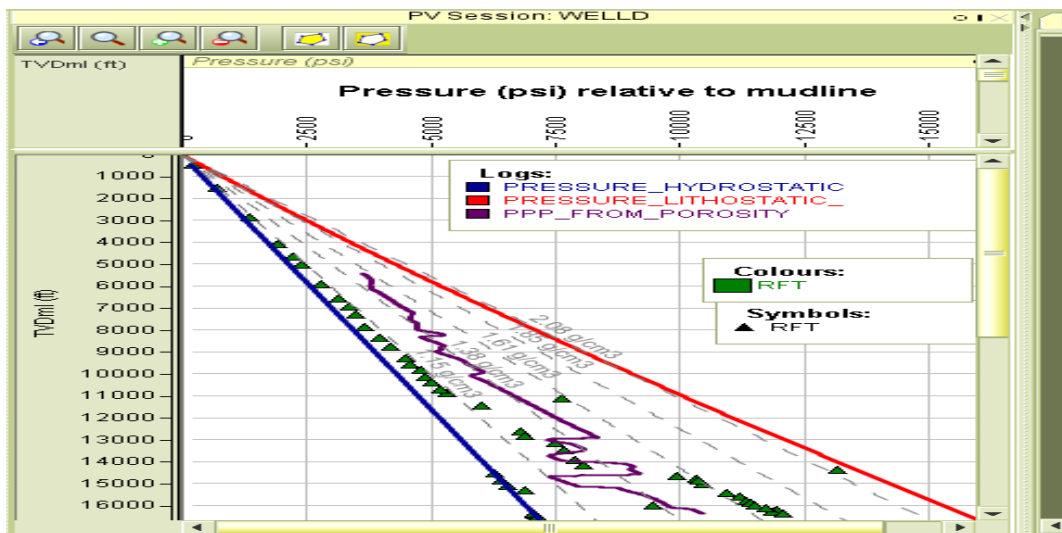


Fig. 11: PPP from Porosity for Well D.

The wavy nature of the pore pressure gradient may be due to a varying volume of quartz within the shale beds which would help in dewatering process. Well D is terminated within this zone of on-setting hard overpressure possibly there was drilling challenges such as mud losses which that were beyond control (drilling information not provided). With the result of prediction from the three models lower than that of measured pore pressure in the overpressured zone, it suggest there was an overbalance drilling to this point.

In well G (Fig. 12), the reading of RFT starts at about 11000ft with hydrostatic status to around a depth of 12000ft where it reads sub-normal (under) pressures and mild overpressures (0.6 to 0.7psi/ft) from 12500ft to the last drilled depth. Predicted pressures compare favourably with the measured pressures; Well G is a much deviated well and mud losses were also reported during the course of well drilling. The sub-normal pressure conditions must have been responsible for these drilling challenges. The fact that the predicted plots are also matching these rather discordant

MPP; the data should be validated and accounted for as it can possibly give clue on mechanisms causing the pressuring and bleed-off occurrence.

Well H (Fig. 13) maintains hydrostatic condition from the beginning to about 9000ft where mild overpressures begin to set in and returns to hydrostatic at 11000ft. Another overpressure regime is observed at about 11600ft and to hard overpressure at terminating depth about 16200ft. The last value of MPP shows a further in-

crease in overpressures down depth; since predictions were done for thick shale beds rather than reservoir sands where the last MPP value was read, this could not be ascertain. However, the porosity-based prediction for this well is in perfect match with the gradient of "Measured Pore Pressure (MPP)".

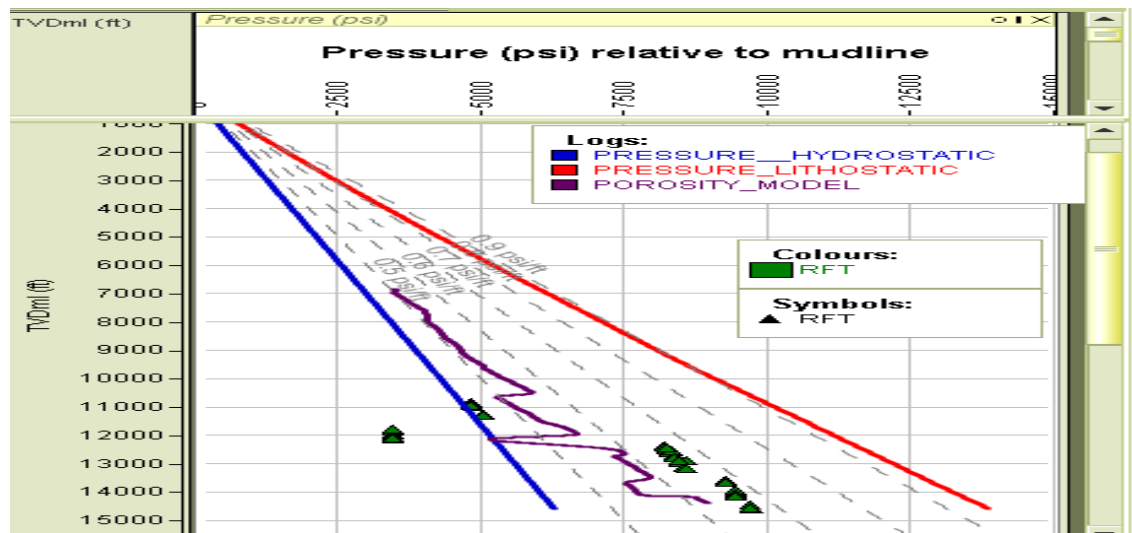


Fig. 12: PPP from Porosity Model for Well G.

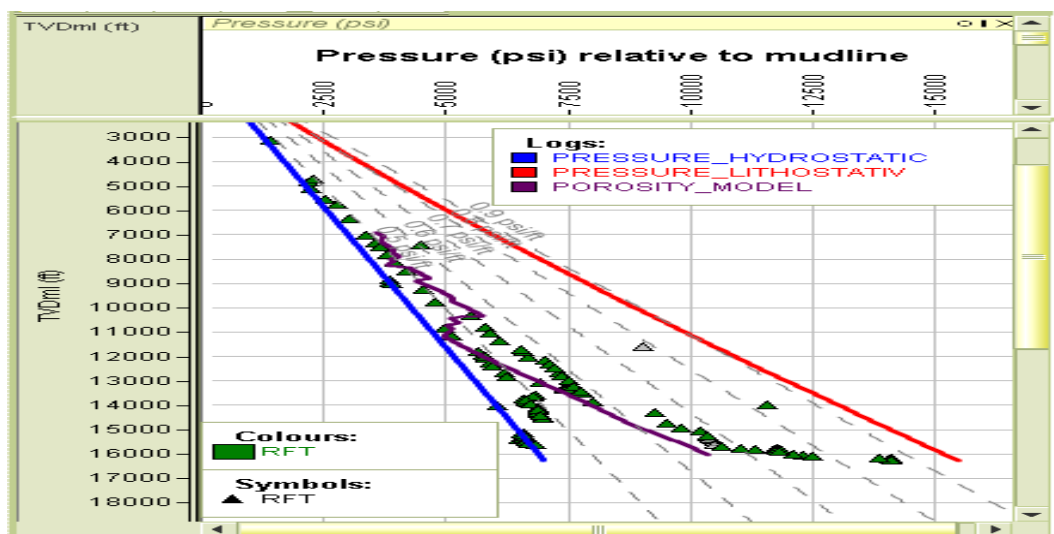


Fig. 13: PPP from Porosity Model for Well H.

And finally in the case study well K (Fig. 14), the result demonstrates hydrostatic pressure down to a depth of about 10,400ft where an "onset of overpressure" is observed. Hard overpressures in the well location exist within the range of 12000ft to 12400ft. Before the overpressure zone, a subnormal pressure zone is also observed. A slight mismatch is however seen between the predicted and measured pressures within these depths range of subnormal pressures.

This could probably be owed to information mix-up in the data provided. Since the mismatch is just not too out of place, the depth range can be put between 8000ft and 11000ft where the subnormal pressures are observed, although this result cannot be validated for future exploration needs unless necessary drilling information is incorporated to these interpretations.

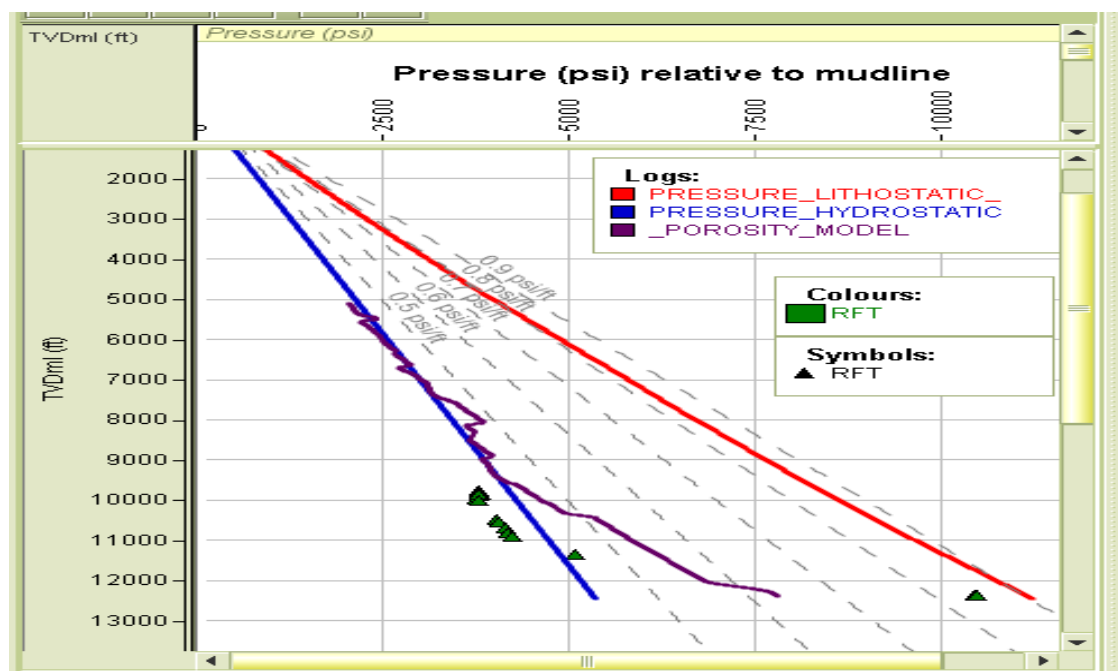


Fig. 14: PPP from Porosity Model for Well K.

## 5. Conclusions

Zones of overpressures have been predicted from the theoretically depth-dependent compaction porosity model. Geopressures are correspondingly higher in thick shale zones with sharp increase in porosity values. The porosity-based prediction model is very suitable to the study area as it yields concordant results with MPPs. These results have successfully met the objectives of this work and are also in agreement with results from similar works in the study area, even with different approaches. Hence, it is recommended for whatever purpose as the reference could be made namely; future exploration works, academic research, economic evaluation and otherwise.

## References

- [1] Bowers, G. L., (1995); Pore Pressure Estimation from Velocity Data: Accounting for Overpressure Mechanisms Besides Undercompaction: *SPE Drilling and Completions*, June, 1–19.
- [2] Carmichael, R. S., (1982); Handbook of Physical Properties of Rocks. *CRC Press Inc*. Boca Rahn, Florida. Vol. 2, 1-228.
- [3] Doust, H., and Omatsola, E., (1990); Niger Delta, in, Edwards, J. D., and Santogrossi, P.A., eds., Divergent/passive Margin Basins, *AAPG Memoir 48: Tulsa, American Association of Petroleum Geologists*, 239-248.
- [4] Eaton, B. A., (1975); the Equation for Geopressure Prediction from Well Logs. *Society of Petroleum Engineers of AIME*, paper SPE 5544. <https://doi.org/10.2118/5544-MS>.
- [5] Flemings, P.B., Stump B.B., Finkbeiner, T. and Zoback, M. (2002); Flow focusing in overpressured sandstones: theory, observations, and applications. *American J. of Science*, Vol. 302, 827–855. <https://doi.org/10.2475/ajs.302.10.827>.
- [6] Holbrook, P.W., Maggiori, D.A., and Hensley, R., (2005); Real-time Pore Pressure and Fracture Gradient Evaluation in all Sedimentary Lithologies. *SPE Formation Evaluation*, Vol. 10, No. 5, 215-222.
- [7] Jiao, J. J. and Zheng, M. V. (1998); Abnormal Fluid Pressures Caused by Deposition and Erosion of Sedimentary Basins. *Journal of Hydrology*, Vol. 13, 124-141. [https://doi.org/10.1016/S0022-1694\(97\)00115-7](https://doi.org/10.1016/S0022-1694(97)00115-7).
- [8] Kumar, B., Niwas, S. and Mangaraj, B.K. (2012); Pore Pressure Prediction from Well Logs and Seismic Data. *9<sup>th</sup> Biennial Intl Conf& Exposition on Pet. Geophy.*
- [9] Short, K.C. & Stauble, A.J., (1967); Outline geology of the Niger Delta. *American Association of Petroleum Geologists Bulletin*, Vol. 5, 761–779.
- [10] Swarbrick, R. E. and Osborne, M.J. (1998); Mechanisms which Generate Overpressure in Sedimentary Basins: a reevaluation. *AAPG Bulletin*, Vol. 81, 1023-1041.
- [11] Tingay, R. P., R. R. Hillis, C. K. Morley, R. C. King, R. E. Swarbrick, and A. R. Damit, (2009); Present-day stress and neotectonics of Brunei: Implications for petroleum exploration and production: *AAPG Bulletin*, Vol. 93, No. 1, 75–100. <https://doi.org/10.1306/08080808031>.
- [12] Traugott, M., (1997); Pore pressure and fracture gradient determinations in deepwater. *World Oil*, August, 815.
- [13] Tuttle, M., Charpentier, R., and Brownfield, M. (2015); the Niger Delta Petroleum System: Niger Delta Province, Nigeria, Cameroon, and Equatorial Guinea, Africa. *United States Geologic Survey*.
- [14] Ugwu, G.Z. (2015); An Overview of Pore Pressure Prediction Using Seismically-Derived Velocities. *Journal of Geology and Mining Research*, Vol. 7, No. 4, 31-40. <https://doi.org/10.5897/JGMR15.0218>.
- [15] Zhang, J. (2011); Pore Pressure Prediction from Well Logs: Methods, Modifications, and New Approaches. *Earth-science Reviews*, Vol. 108, 50-63. <https://doi.org/10.1016/j.earscirev.2011.06.001>.
- [16] Zijian, C., Jingen, D., Baohua, Y., Qiang, T., and Zhuo, C. (2015); the Improvement Methods of Pore Pressure Prediction Accuracy in the Central Canyon in Qiongdongnan Basin. *IPCBE*, Vol. 85, No. 1.

## Appendix: Tables

**Table 1:** Calculated Porosities (Well A)

Depth (ftTVDml)	Shale Velocity (ft/s)	Shale Porosity (fract.)
3000.0	6393.11	0.69
3200.0	6443.62	0.65
3400.0	6566.21	0.55
3600.0	6748.22	0.55
4000.0	7239.91	0.65
4400.0	7817.46	0.58
4600.0	8106.79	0.54
4800.0	8379.64	0.49
5000.0	8623.33	0.44
5200.0	8825.22	0.4
5400.0	8972.66	0.37
5600.0	9052.99	0.35
5800.0	9041.53	0.32
6000.0	8863.6	0.3
6200.0	8670.88	0.37
6400.0	8757.09	0.42
6600.0	8955.53	0.36
6800.0	9092.68	0.34
7000.0	9337.12	0.32
7200.0	9573.96	0.26
7400.0	10230.66	0.25
7600.0	9299.6	0.27
7800.0	9661.56	0.30
8000.0	9144.27	0.33
8200.0	8818.83	0.35
8400.0	8980.66	0.33
8600.0	9502.23	0.33
8800.0	8920.71	0.33
9000.0	9058.74	0.33
9200.0	10684.49	0.22
9400.0	10143.35	0.22
9600.0	10241.51	0.21
9800.0	9974.77	0.24
10000.0	10226.57	0.21
10200.0	9600.85	0.21
10400.0	11214.82	0.24
10600.0	10533.23	0.27
10800.0	9569.16	0.28
11000.0	9556.85	0.28
11200.0	10340.07	0.28
11400.0	9828.61	0.26
11600.0	9866.27	0.26
11800.0	10331.23	0.25
12000.0	10889.53	0.25

**Table 2:** Calculated Porosities (Well B)

Depth (ftTVDml)	Shale Velocity (ft/s)	Shale Porosity (fract.)
8599.83	8434.63	0.31
8799.83	9192.86	0.29
8999.83	8110.16	0.25
9199.83	9723.92	0.21
9399.83	10065.33	0.18
9599.83	10353.45	0.16
9799.83	9531.89	0.17
9999.83	10059.41	0.19
10199.83	9922.92	0.19
10399.83	10532.79	0.15
10599.83	11108.34	0.15
10799.83	10300.17	0.15
10999.83	10580.13	0.15
11199.83	11067.81	0.14
11399.83	10364.39	0.14
11599.83	10553.82	0.14
11799.83	11233.74	0.14
11999.83	10717.85	0.14
12199.83	11028.12	0.14
12399.83	10900.13	0.13
12599.83	11562.79	0.13
12799.83	11718.39	0.12
12999.83	11907.18	0.11
13199.83	11815.11	0.11
13399.83	10767.52	0.1

13599.83	11228.08	0.09
13799.83	12468.67	0.08
13999.83	12704.38	0.08
14199.83	12887.1	0.07
14399.83	12315.08	0.07
14599.83	13308.75	0.06
14799.83	12636.2	0.05
14999.83	12896.15	0.05
15199.83	13372.52	0.04
15399.83	11163.01	0.05
15599.83	11641.16	0.09

**Table 3:** Calculated Porosities (Well D)

Depth (ftTVDml)	Shale Velocity (ft/s)	Shale Porosity (fract.)
5600.0	7249.24	0.44
5800.0	7507.38	0.41
6000.0	7829.88	0.37
6200.0	7968.77	0.35
6400.0	7985.61	0.35
6600.0	8036.25	0.34
6800.0	8092.69	0.33
7000.0	8127.42	0.33
7200.0	8175.28	0.32
7400.0	8559.13	0.29
7600.0	8805.99	0.27
7800.0	8916.51	0.26
8000.0	9173.97	0.23
8200.0	8731.04	0.27
8400.0	9597.6	0.21
8600.0	9453.52	0.22
8800.0	9667.37	0.2
9000.0	10012.46	0.18
9200.0	9906.4	0.18
9400.0	9824.69	0.19
9600.0	9908.32	0.19
9800.0	9912.59	0.18
10000.0	10200.52	0.17
10200.0	10470.28	0.15
10400.0	10433.08	0.15
10600.0	10440.1	0.15
10800.0	10456.45	0.15
11000.0	10480.17	0.15
11200.0	10509.3	0.15
11400.0	10541.87	0.15
11600.0	10575.94	0.14
11800.0	10609.53	0.14
12000.0	10640.68	0.14
12200.0	10667.43	0.14
12400.0	10687.82	0.14
12600.0	10699.89	0.14
12800.0	10698.64	0.14
13000.0	11912.47	0.08
13200.0	11593.96	0.09
13400.0	11563.04	0.09
13600.0	12000.15	0.07
13800.0	12326.6	0.06
14000.0	12030.38	0.07
14200.0	11382.78	0.10
14400.0	11612.21	0.09
14600.0	11920.81	0.08
14800.0	12857.95	0.04
15000.0	12792.95	0.04
15200.0	12386.88	0.06
15400.0	12316.7	0.06
15600.0	12223.89	0.06
15800.0	12221.78	0.06
16000.0	12250.82	0.06
16200.0	12004.78	0.07

**Table 4:** Calculated Porosities (Well G)

Depth (ftTVDml)	Shale Velocity (ft/s)	Shale Porosity (fract.)
6945.32	8637.68	0.22
7145.32	8664.07	0.22
7345.32	8704.9	0.22
7545.32	8702.95	0.22
7745.32	8857.34	0.21
7945.32	9104.3	0.19
8145.32	9187.82	0.18
8345.32	9288.34	0.18
8545.32	9430.92	0.17
8745.32	9465.78	0.17
8945.32	9572.82	0.16
9145.32	9710.85	0.15
9345.32	9753.88	0.15
9545.32	9767.69	0.15
9745.32	9856.76	0.15
9945.32	9854.8	0.15
10145.32	9830.09	0.15
10345.32	9806.43	0.15
10545.32	10011.49	0.14
10745.32	10714.66	0.11
10945.32	10770.5	0.10
11145.32	10754.59	0.11
11345.32	10775.94	0.11
11545.32	10782.56	0.10
11745.32	10555.5	0.11
11945.32	10529.64	0.11
12145.32	11994.29	0.09
12345.32	11230.93	0.09
12545.32	10349.16	0.12
12745.32	10688.78	0.11
12945.32	10682.85	0.11
13145.32	10708.01	0.11
13345.32	10741.35	0.11
13545.32	10937.19	0.10
13745.32	11401.77	0.08
13945.32	11453.94	0.08
14145.32	11100.84	0.09
14345.32	10685.57	0.11

**Table 5:** Calculated Porosities (Well H)

Depth (ftTVDml)	Shale Velocity (ft/s)	Shale Porosity (fract.)
6999.86	8697.93	0.22
7199.86	8982.0	0.20
7399.86	9133.51	0.19
7599.86	9182.62	0.19
7799.86	9402.3	0.17
7999.86	9802.16	0.15
8199.86	10200.36	0.13
8399.86	9752.85	0.16
8599.86	9725.09	0.16
8799.86	9707.25	0.16
8999.86	10179.19	0.13
9199.86	10078.21	0.14
9399.86	10060.34	0.14
9599.86	10128.65	0.14
9799.86	10301.18	0.13
9999.86	10244.09	0.13
10199.86	10210.34	0.13
10399.86	11083.98	0.09
10599.86	11099.05	0.09
10799.86	11502.09	0.08
10999.86	11677.37	0.07
11599.86	11867.14	0.06
12399.86	11786.21	0.06
12599.86	11755.91	0.06
12799.86	11723.78	0.06
12999.86	11690.9	0.07
13199.86	11658.36	0.07
13399.86	11627.27	0.07
13599.86	11598.7	0.07
14399.86	11531.59	0.07
14599.86	11527.46	0.07
14799.86	11500.45	0.07
14999.86	11451.17	0.07
15199.86	11389.58	0.08
15399.86	11325.62	0.08
15599.86	11269.25	0.08
15799.86	11230.43	0.08
15999.86	11217.4	0.08

**Table 6:** Calculated Porosities (Well K)

Depth (ftTVDml)	Shale Velocity (ft/s)	Shale Porosity (fract.)
5199.85	8701.59	0.21
5399.85	8769.68	0.21
5599.85	8999.43	0.19
5799.85	9029.28	0.19
5999.85	9135.6	0.18
6199.85	9227.25	0.18
6399.85	9348.85	0.17
6599.85	9350.3	0.17
6799.85	9599.87	0.15
6999.85	9559.46	0.15
7199.85	9656.74	0.15
7399.85	9759.11	0.14
7599.85	9600.39	0.15
7799.85	9637.81	0.15
7999.85	9634.94	0.15
8199.85	10042.7	0.12
8399.85	10196.15	0.11
8599.85	10341.33	0.10
8799.85	10359.26	0.10
8999.85	10624.2	0.09
9199.85	10703.06	0.09
9399.85	10787.65	0.08
9599.85	10718.71	0.09
9799.85	10704.13	0.09
9999.85	10707.97	0.09
10199.85	10674.0	0.09
10399.85	10424.19	0.10
10599.85	10366.11	0.10
10799.85	10373.27	0.10
10999.85	10381.56	0.10
11199.85	10371.09	0.10
11399.85	10361.15	0.10
11599.85	10357.75	0.11
11799.85	10343.81	0.11
11999.85	10333.49	0.11
12199.85	9856.43	0.13